Global and Planetary Change 253 (2025) 104975

Contents lists available at ScienceDirect

Global and Planetary Change

journal homepage: www.elsevier.com/locate/gloplacha

A Late Glacial and Holocene sugar biomarker-based $\delta^{18}O$ paleoclimate record from the Afro-alpine Central Lake, Bale Mountains, Ethiopia

Samuel G. Chernet [a,b,*], Lucas Bittner [a], Graciela Gil-Romera [c], Bruk Lemma [d], Marcel Bliedtner [e], Roland Zech [e], Bruno Glaser [f], Tobias Bromm [f], Sönke Szidat [g], Wolfgang Zech [h], Michael Zech [a]

[a] Physical Geography, TU Dresden, 01069 Dresden, Germany
[b] School of Earth Sciences, Addis Ababa University, P.O. Box 1176, Addis Ababa, Ethiopia
[c] Department of Geo-environmental Processes and Global Change, Pyrenean Institute of Ecology, CSIC, 50059 Zaragoza, Spain
[d] Institute of Geological Sciences, Freie Universität Berlin, Malteserstrasse 74-100, 12249 Berlin, Germany
[e] Institute of Geography, Friedrich Schiller University of Jena, Jena, Germany
[f] Institute of Agronomy and Nutritional Sciences, Soil Biogeochemistry, Martin-Luther-University Halle-Wittenberg, 06108 Halle (Saale), Germany
[g] Department of Chemistry, Biochemistry and Pharmaceutical Sciences & Oeschger Centre for Climate Change Research, University of Bern, Bern, Switzerland
[h] Department of Soil Science, University of Bayreuth, Germany

ARTICLE INFO

Editor: Dr. Sun Jimin

Keywords:
Biomarkers
Oxygen isotopes
Hydroclimate
Ethiopian Highlands
East Africa
Afro-alpine climate

ABSTRACT

The Eastern African region is an amalgamation of complex climate systems nestled in contrasting topographic barriers. Although rift basins are prime targets for studying the climate of the past, high-altitude climate archives in the context of paleoclimate research also offer invaluable insight and have yet to be fully explored. Here, we present a 17 kyr hydroclimate history of the Afro-alpine (4121 m a.s.l) Central Lake using a $\delta^{18}O$ record established by analyzing hemicellulose-derived sugar biomarkers. The sugar biomarker patterns with a dominance of fucose indicate the predominance of autochthonous sedimentary organic matter. Therefore, the oxygen isotopic variability of the sugar biomarkers in general and of fucose in particular ($\delta^{18}O_{fucose}$) reflects $\delta^{18}O_{lake\ water}$ being controlled by climatic conditions, particularly lake water ^{18}O enrichment by evaporation. Our $\delta^{18}O_{fucose}$ record from Central Lake indicates strong enrichment during the Late Glacial. Around 15 cal kyr BP, the onset of more humid climate marks the beginning of the African Humid Period (AHP) in the Bale Mountains. The AHP was interrupted by an arid period during the Late Glacial – Holocene transition roughly coinciding with the Younger Dryas (YD). After the YD, humid climatic conditions prevailed again until the Late Holocene when a gradual shift towards drier climate started. Our $\delta^{18}O_{fucose}$ record and interpretation agree well with the findings from adjacent low-altitude archives of Eastern Africa, the Indian Ocean paleoclimate records and the Asian Monsoon Domain, which suggests region-wide hydro-climatic teleconnections.

1. Introduction

Several paleoclimate studies show the interplay between various climate forcings and the spatiotemporal climate complexity of Eastern Africa since the Last Glacial Maximum (LGM) (Stager et al., 2002; Liu et al., 2018). These climate records outline orbital forced long term climate change (e.g., Tierney et al., 2008; Schaebitz et al., 2021) or the strength of various monsoon systems and the latitudinal movement of the tropical rain belt (e.g., Fleitmann et al., 2003; Stager et al., 2011; Weldeab et al., 2014; Meyer et al., 2020). Some records also indicate the influence of polar ice surges like Heinrich events (HE) and the Younger Dryas (YD) on weakening tropical hydroclimate dynamics (Weldeab et al., 2005; Jung et al., 2009; Mohtadi et al., 2014; Liu et al., 2018).

Untangling the driving mechanisms of long and short-term climate variability in this region is challenging for several reasons. These include (i) a limited number of studied terrestrial paleoclimate archives, (ii) differences in sensitivity, thresholds, and timing of proxies used to detect paleoclimate shifts, possibly affecting interpretation (Castañeda et al., 2016) and, (iii) the complex interaction of regional and global hydroclimate systems coupled with the juxtaposition of highland and

* Corresponding author at: Physical Geography, TU Dresden, 01069 Dresden, Germany.
E-mail address: samuel_getachew.chernet@tu-dresden.de (S.G. Chernet).

https://doi.org/10.1016/j.gloplacha.2025.104975
Received 21 March 2025; Received in revised form 4 July 2025; Accepted 6 July 2025
Available online 8 July 2025

East African Rift microclimatic conditions (Trauth et al., 2010; Junginger et al., 2014) that complicate high-resolution climate reconstruction in this region.

During the last decades, the urgent need to understand how climate operated in the past and its implication for future climate change has pushed the frontiers of paleoclimate studies.

One example is the development and application of molecular patterns and isotopic signatures of hemicellulose-derived sugar biomarkers in paleoclimate studies (e.g. Jia et al., 2008; Zech et al., 2013, 2014b; Hepp et al., 2016; Duan et al., 2017; Benettin et al., 2018; Bittner et al., 2022).

The ubiquity of sugar biomarkers in the terrestrial and aquatic biosphere, their source-specific nature, and their linkage to specific environmental processes make them a prime candidate for the study of climate-biosphere interactions (Jia et al., 2008; Hepp et al., 2016; Holtvoeth et al., 2019). Allochthonous inorganic molecules are used by photosynthetic and chemoautotrophic communities to produce biomass. Hence, biomass's isotopic composition often reflects the reservoir's variabilities modified by fractionation during metabolism (Holtvoeth et al., 2019). The $\delta^{18}O$ composition of aquatic cellulose experiences a fractionation of about +29 ‰ compared to the $\delta^{18}O$ composition of the lake water (Mayr et al., 2015). A similar fractionation factor was observed for terrestrial hemicellulose-derived sugar biomarkers (Zech et al., 2014a; Hepp et al., 2021). Regarding post-depositional processes potentially biasing the environmental $\delta^{18}O_{sugar}$ signals, Zech et al. (2012) showed that $\delta^{18}O$ of plant-derived sugar biomarkers are not affected by fractionation during decomposition and litter formation, which makes them suitable for paleoclimate studies.

Hemicellulose-derived sugar biomarkers were used for the Holocene paleoclimate reconstruction of Lake Garba Guracha in the Bale Mountains (Fig. 1; Bittner et al., 2020; Bittner et al., 2022). In both studies, the effectiveness of sugar biomarker proxies was compared to conventional proxies, including charcoal and pollen (Umer et al., 2007; Gil-Romera et al., 2019), diatoms, sedimentology/mineralogy, and organic chemistry (Tiercelin et al., 2008). The Holocene sugar biomarker records were consistent with other proxies despite differences in proxy response to environmental factors (Bittner et al., 2022).

In the present study, we aim to apply sugar biomarkers to another lake in the Bale Mountains,namely the neighboring Central Lake, situated on the Sanetti Plateau ~150 m higher than Garba Guracha. Our specific aims and questions are (i) establishment of a robust chronostratigraphy for Central Lake, (ii) aquatic versus terrestrial source identification of the sugar biomarkers, (iii) establishment of a $\delta^{18}O_{sugar}$ record for Central Lake, thus also extending the $\delta^{18}O_{sugar}$ record of Garba Guracha into the Late Glacial and (iv) paleoclimatic interpretation of the $\delta^{18}O_{sugar}$ record for Central Lake and comparison with existing records from the Bale Mountains as well as with other East African records.

2. Study area

Central Lake (06° 51′16.1″ N/ 39° 52′ 56.1″ E) is an Afro-alpine lake located in one of Africa's most extensive and contiguous mountains, the Bale-Arsi Massief (Kidane et al., 2012; Eggermont et al., 2011; Fig. 1). It was formed due to episodic volcanism during the Miocene, Pliocene, and Quaternary periods associated with the breakup of Afro-Arabian plates and the formation of the East African Rift system (Nelson et al., 2019). The Bale Mountains National Park is the largest alpine ecosystem in Africa (Mekonnen et al., 2022). Notable physiographic features include the 600 km^2 Sanetti Plateau with the country's second tallest peak, Mount Tulu Dimtu, at 4377 m a.s.l (Fig. 1). The topmost part of the plateau consists of horizontally bedded lava flows of trachytic and basaltic composition (Osmaston et al., 2005; Nelson et al., 2019). The plateau is bordered by a steep escarpment to the south and has deeply incised valleys with northward draining rivers (Tiercelin et al., 2008). The plateau and valleys were extensively glaciated during the Last

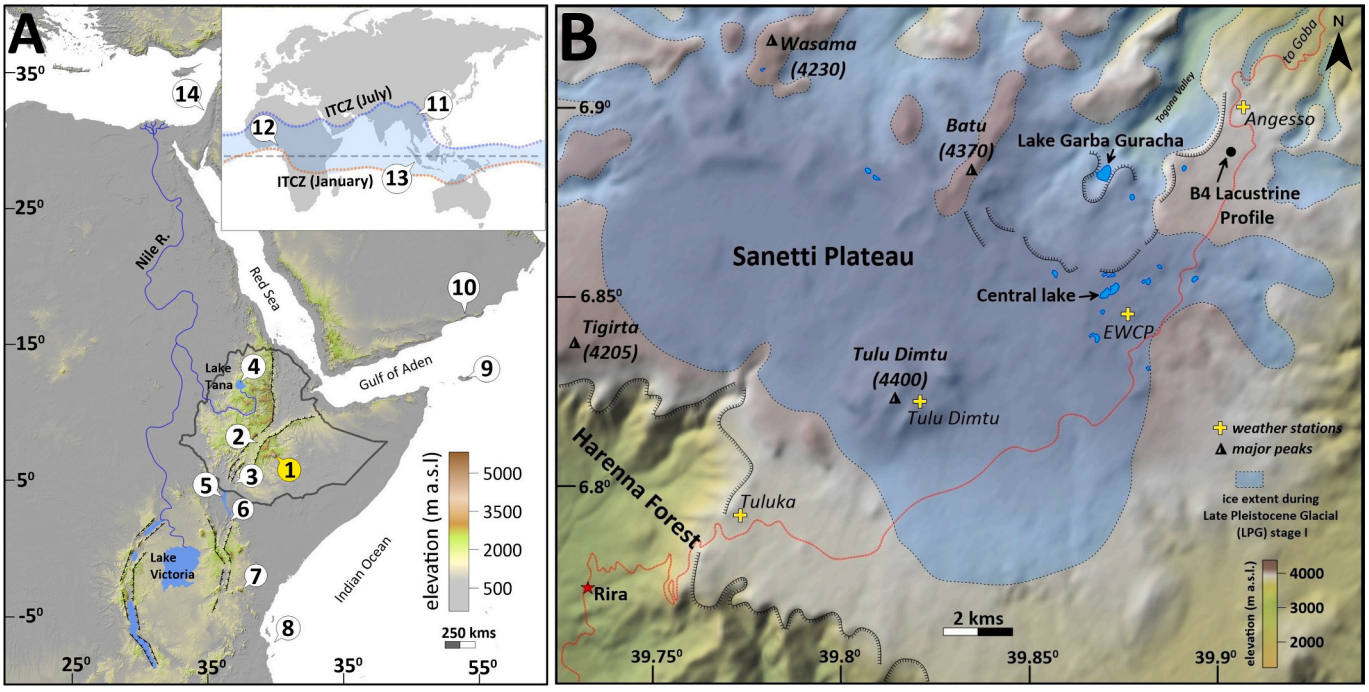

Fig. 1. (**A**) Locations of archives referred to in this work; 1- Bale Mountains (this study); 2- Ziway-Shala Basin (Gillespie et al., 1983); 3-Chew Bahir Basin (Foerster et al., 2012); 4-Lake Tana (Marshall et al., 2011); 5- Lake Turkana (Garcin et al., 2012); 6- paleo-Lake Suguta (Junginger et al., 2014); 7- Kilimanjaro Ice core records (Thompson et al., 2002); 8- Marine core record GeoB12615–4 (Romahn et al., 2014); 9- Stalagmite M1–5 from Socotra Island (Shakun et al., 2007);10- Qunf Cave (Fleitmann et al., 2003); 11- Dongge cave (Dykoski et al., 2005); 12- Lake Bosumtwi (Shanahan et al., 2006); 13- core 39 KL in eastern Indian Ocean (Mohtadi et al., 2014); 14- SL112 core registering Nile river runoff (Weldeab et al., 2014). (**B**) Topographic map of the Bale Mountains and location of Central Lake, Garba Guracha (Bittner et al., 2020; Bittner et al., 2022) and B4 (Mekonnen et al., 2022). Ice cap reconstruction during Late Pleistocene Glacial (LPG Stages I-III, 35.1 + 7.1 to 16 + 1 cal kyr BP, Groos et al., 2021).

Glacial Maximum (Osmaston et al., 2005; Groos et al., 2021). Extensive wetlands and lakes formed after deglaciation around 18 cal kyr BP (Mekonnen et al., 2022). Central Lake has an area of 0.1 km^2 with 0.8 m water depth, yet highly variable depending on the season, and a very small catchment.

Modern climate of Eastern Africa is influenced by the West African Monsoon (WAM) and Indian Ocean Monsoon (IOM) (Camberlin, 1997; Kebede and Travi, 2012; Costa et al., 2014; Junginger et al., 2014). These monsoon systems and the latitudinal movement of the Inter Tropical Convergence Zone (ITCZ) control the seasonal and multi-annual rainfall pattern throughout the region (Nicholson, 2000; Baker et al., 2007; Tierney and Russell, 2007; Lamb et al., 2018; Lemma et al., 2020).

The present-day climate in the Bale Mountains has an 8-month long wet season with bimodal precipitation pattern (March to October) followed by a 4-month dry season from November to February (Seleshi and Zanke, 2004; Lemma et al., 2020). The orographic setup of the region enables a prolonged and high rainfall amount compared to areas of similar latitude in the continent (Kebede and Travi, 2012). Due to its proximity to the Indian Ocean and the Arabian Sea, this region receives more than 50 % of its moisture directly from these regions (Lemma et al., 2020; Stojanovic et al., 2022).

Modern vegetation in the Bale Mountains is orographically grouped into an Afromontane forest belt (1400–3000 m a.s.l; e.g., *Podocarpu falcatus, Allophylus abyssinicus, Juniperus procera and Hagenia abyssinica*) followed by the Ericaceous belt (3000–3800 m a.s.l; e.g., *Erica arborea* and *Erica timera*) and an Afro-alpine belt (>4000 m a.s.l; e.g., *Lobelia, Alchemilla and Poaceae*) (Friis, 1986; Miehe and Miehe, 1994; Lemma et al., 2019; Umer et al., 2007; Mekonnen et al., 2019). Pollen records from surrounding lakes document past vegetation change in response to climate change (cf., Tiercelin et al., 2008; Gil-Romera et al., 2021; Mekonnen et al., 2022) and anthropogenic influence (Gil-Romera et al., 2019).

3. Material and methods

3.1. Sampling and dating

Sediment samples from up to 4.81 m depth were retrieved from the shoreline of Central Lake using an Edelman- and a Pürckhauer corer. Although the coring did not reach bedrock, the increasing presence of rock fragments towards the lower section suggests proximity. Core description and sampling were conducted in the field. For this study, we focus on fine-grained sediments down to 410 cm depth (Fig. 2). Samples were air-dried and stored in plastic bags for transport.

A total of 12 bulk sediment samples were analyzed to establish a radiocarbon-based (^{14}C) chronology using an Accelerator Mass Spectrometry (AMS) and an elemental analyzer (Vario MICRO cube from Elementar) at the Laboratory for the Analysis of Radiocarbon with AMS (LARA) at the University of Bern (Szidat et al., 2014). These radiocarbon ages were subsequently used to construct an age-depth model with rBacon (version 3.1.1) and IntCal20 Northern Hemisphere calibration (Reimer et al., 2020), in RStudio (version 4.2.3), following the method outlined by Blaauw and Christen (2011) (Fig. 2).

3.2. Inorganic geochemical analysis

Forty-three samples were analyzed for major and trace elements using Bruker S8 Tiger Wavelength Dispersive X-ray Fluorescence (WD-XRF) at Soil Science and Protection, Martin Luther University, Halle-Wittenberg, Germany. The samples were carbonate-free and dried at 105 °C before analysis. Results were corrected for soil and sediment organic matter using Eq. (1).

$$\%x_{corrected} = \%x_{measured} * \left[\frac{100}{100 - \%GV_{1000} - \%H_2O}\right] \quad (1)$$

where 'X' is elemental concentration in percent and GV_{1000} is mass loss on ignition at 1000 °C.

A centered log-ratio transformation was performed to reduce matrix

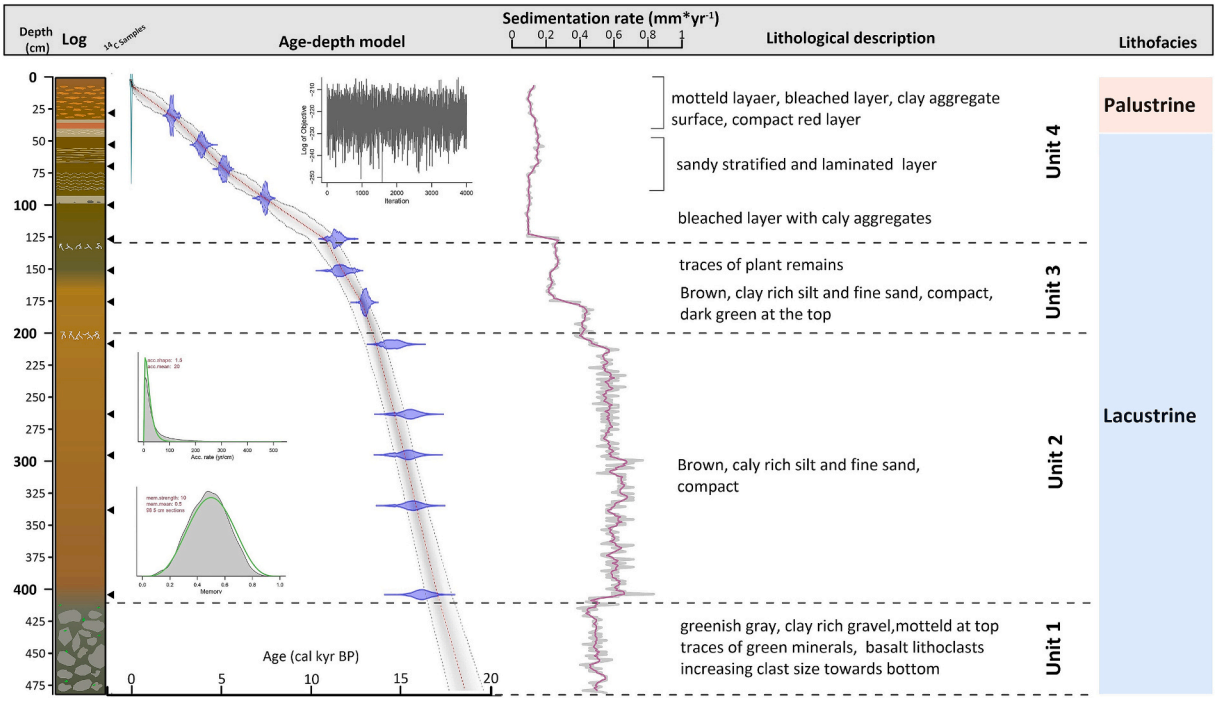

Fig. 2. Description of the retrieved core, samples for ^{14}C dating in stratigraphic position (cf. Table 1) along with age-depth model using the R-Bacon package of Blaauw and Christen (2011) and modeled sedimentation rate (grey line shows value per cm while the purple line shows running mean of 5). (For interpretation of the references to colour in this figure legend, the reader is referred to the web version of this article.)

effects (Bertrand et al., 2024) and perform principal component analysis (PCA). The optimal number of clusters were determined using the elbow method (Zhang et al., 2024), K-means of clustering was then applied to the first two PCA scores.

3.3. Elemental analysis

Total Organic Carbon (TOC $n = 62$) and nitrogen (N) were measured using an Elementar Analyzer (Vario EL cube) coupled to an isotope ratio mass spectrometer (Isoprime precision) at Friedrich Schiller University Jena. Samples were treated with HCl (10 %) at 60 °C for 8 h and washed with ultrapure water to eliminate carbonate minerals. Ten milligram of sediment was weighed and placed in tin boats for $\delta^{13}C$ measurement. The accuracy of the $\delta^{13}C$ analyses was confirmed by co-analyzing certified standards (L-Prolin, EDTA, and USGS65), achieving analytical uncertainties of less than 0.1 ‰. All $\delta^{13}C$ values are expressed in delta notation relative to the Vienna Pee Dee Belemnite (VPDB). The molar TOC/N ratio was calculated as molar TOC/N = (TOC*12.0107)/(N*14.0067) (Strobel et al., 2022).

3.4. Biomarker extraction and analysis

A total of 29 samples were chosen for sugar biomarker analysis. Samples were hydrolyzed in 4 M trifluoroacetic acid at 105 °C for four hours. 100 µg of Myo-inositol was added to each sample as an internal standard for the extraction process. The solution was then filtered and purified using glass fiber filters, XAD 7 and DOWEX 50WX8 columns (Amelung et al., 1996). Aliquots of the sugar extracts were mixed with 200 mL pyridine and methylboronic acid (MBA) for compound-specific stable isotope analysis and derivatized for 1 h at 60 °C (Zech and Glaser, 2009). Derivatives were measured in triplicate using a Trace GC 200 coupled with Delta V Advantage IRMS. Corrections for possible amount dependency, the effect of exchangeable oxygen atoms of the carbonyl groups (Zech and Glaser, 2009), and instrument drift were done post-analysis. Results are presented using the δ-notation versus Vienna Standard Mean Ocean Water (VSMOW). The mean standard errors for triplicate analyses were 0.55 ‰, 0.44 ‰, and 0.45 ‰ for arabinose, fucose, and xylose, respectively.

Aliquots for quantification were derivatized with 200 µl *N*-methyl-pyrrolidone (NMP) and *O*-methyl hydroxylamine at 75 °C for 30 min, followed by a five-minute derivatization after the addition of 400 µl of *N*, *O*-Bis(trimethylsilyl)trifluoroacetamide (BSTFA). 5α-androstane was added as a second internal standard. The *O*-methyloxime trimethylsilyl derivatives were separated on a Shimadzu GC 2010 gas chromatograph (Shimadzu, Kyoto, Japan) and detected by flame ionization detector (FID). A Supelco SPB-5 fused silica capillary column (30 m × 0.2 mm inner diameter; 0.2 µm film thickness) was used. Two outliers at 1.3 and 1.7 m depth were excluded from further data evaluation because recovery problems led to anomalously high sugar values (Table S1). All extraction and measurements were done at the Institute of Geography, Technical University of Dresden.

4. Results

4.1. Chronology and lithostratigraphy

The age-depth model shows that Central Lake represents a more or less continuous ~17 cal kyr BP environmental archive (Table 1; Fig. 2). The average sedimentation rate for whole core is 0.41 mm yr^{-1}.The variations in sedimentation rate, grain size analysis, and field-based descriptive textural and sedimentological properties enable the classification of the core into four lithostratigraphic units (Figs. 2 & 3).

Unit 1 (481 to 410 cm, >17 cal kyr BP) comprises a gravel layer with a dark grey clay matrix, lithoclasts (basaltic in composition), and associated green minerals (likely olivine). Grain size increases with depth. The mean sedimentation rate for this unit is 0.5 mm yr^{-1}.

Table 1
AMS radiocarbon data on total organic matter (bulk sediment) from Central Lake. Calibrated ages along with their 2-σ range calculated using R-Bacon package (version 4.2.3) (Blaauw and Christen, 2011).

Sample no.	Sample Depth *(cm)*	^{14}C age	Calibrated age *(cal. BP, 2σ range)*	Calibrated median age *(cal. BP,* min /max*)*
BEnr.16132.1.1	28	2260 +81	2024–2480	2212 (*1903/2594*)
BEnr.13642.1.1	51	3597 +112	3601–4225	3900 (*3544/4294*)
BEnr.16133.1.1	70	4512 +97	4864–5448	5170 (*4861/5515*)
BEnr.13643.1.1	100	6553 +136	7206–7686	8100 (*7446/9042*)
BEnr.16134.1.1	125	9895 +142	10,933–11,893	10,786 (*9872/11348*)
BEnr.13644.1.1	150	10,072 +195	11,051–12,363	11,742 (*11,215/12330*)
BEnr.16135.1.1	175	11,103 +153	12,731–13,287	12,839 (*12,106/13135*)
BEnr.13645.1.1	208	12,372 +256	13,691–15,387	12,624 (*13,005/14097*)
BEnr.13646.1.1	263	12,886 +271	14,401–16,265	14,621 (*14,107/15191*)
BEnr.13647.1.1	295	12,972 +276	14,584–16,384	15,185 (*14,638/15723*)
BEnr.13648.1.1	335	13,070 +281	14,756–16,524	15,820 (*15,276/16375*)
BEnr.13649.1.1	405	13416 +268	15,364–16,980	16,983 (*16,375/17813*)

Unit 2 (410 to 197 cm, 17–13.3 cal kyr BP) is composed of brownish-grey coarse silt rich in clay. Grain size analysis indicates 20–40 % sand (Fig. 3). Unit 2 is compact and lacks any discernable sedimentary structures. The age-depth model yields the highest sedimentation rate of the archive (0.6 mm yr^{-1}) for this unit.

Unit 3 (197 to 128 cm, 13.3–10.7 cal kyr BP) is composed of brownish-grey clay-rich silt at the bottom that gradually changes to dark greenish grey towards the top. Unit 3 is bounded by layers containing traces of plant material. The sand content significantly decreases compared to Unit 2 (Fig. 3). The sedimentation rate changes stepwise from 0.2 to 0.4 mm yr-1 between 160 and 180 cm and 180–197 cm depth (Fig. 2).

Unit 4 (128 to 0 cm, 10.7 cal kyr BP-present) comprises greenish to dark brownish-grey fine sand-rich silt and clay layers. Unlike Unit 2 and 3, Unit 4 is layered and shows different sedimentary structures. The bottom to top, (i) a 25 cm is a massive bed with no sedimentary structures that is overlain by a bleached layer (4 cm) containing clay aggregates (ii) a 50 cm laminated layer overlain by a 14 cm bleached layer containing laminated red layers and (iii) a 35 cm mottled clay-rich coarse silt layer (Fig. 2). The sand content of Unit 4 is higher and more variable than in Unit 2 and 3 (Fig. 3). Unit 4 has the lowest sedimentation rate in the record, with an average sedimentation rate of 0.1 mm yr^{-1}.

4.2. Inorganic geochemistry

In comparison with Post-Archean Australian shales (PAAS) and Upper continental crust (UCC) considered as an average composition of the upper crust (Taylor and McLennan, 1995; Rudnick and Gao, 2003), the analyzed samples have lower SiO_2, Al_2O_3, K_2O, CaO, Na_2O, values and higher TiO_2, Fe_2O_3 values (Table S3). Principal Component Analysis (PCA) shows distinct compositional groupings across the sediment record (Fig. 3A). The first two principal components explain 59.9 % of the total variance (PC1: 41.3 %, PC2: 18.6 %). PC1 primarily clusters samples based on SiO_2 and Zr loading negatively and CaO, MgO, Sr, and TiO_2 loading positively. Fe_2O_3, P_2O_5, and MnO influence PC2. Sample clusters broadly correspond to temporal phases: Cluster 1 (0–7.6 cal kyr BP)

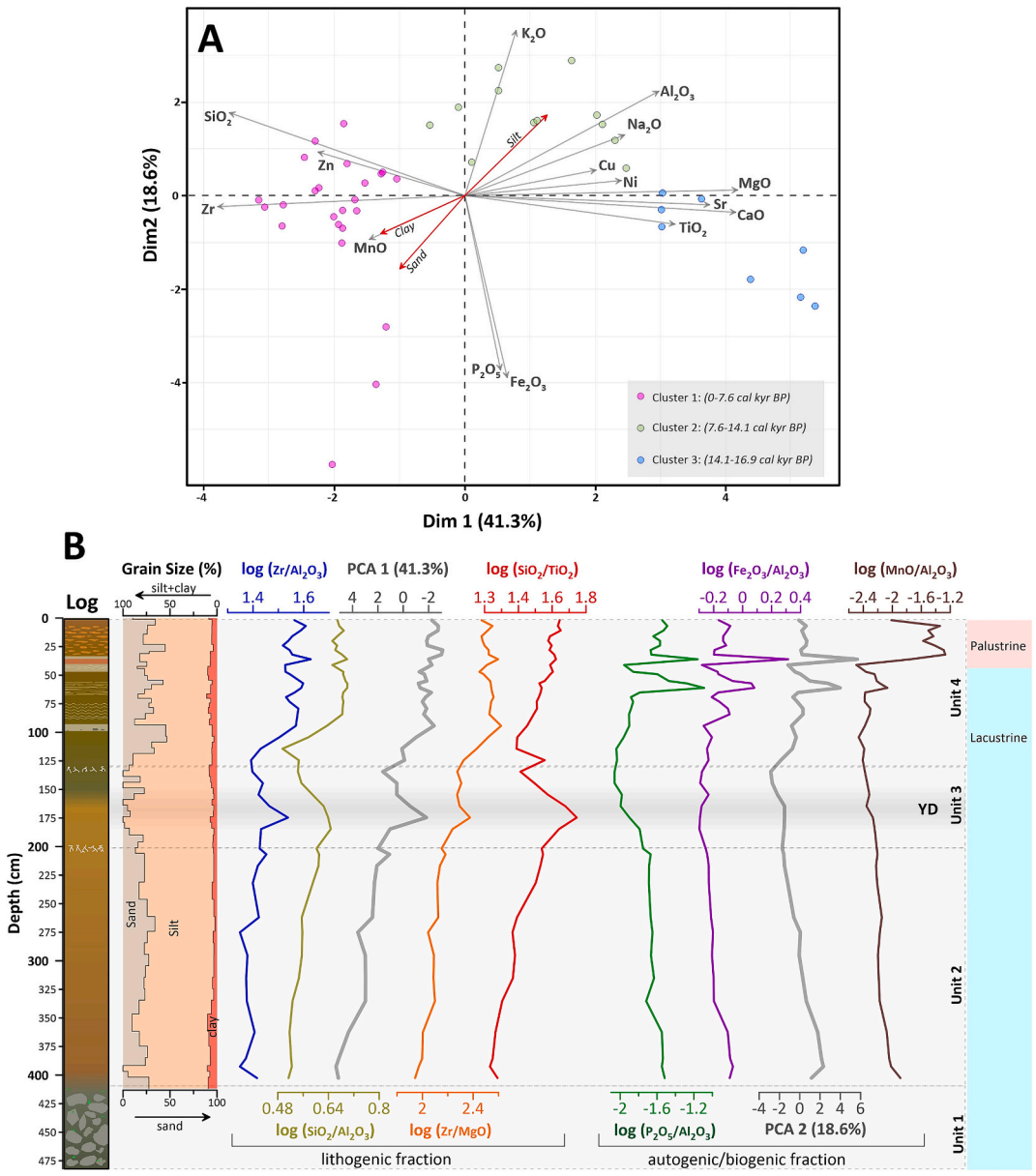

Fig. 3. Geochemical analysis of sediments (**A**) PCA biplot of centered log-ratio (CLR)-transformed geochemical data from lake sediment samples (Bertrand et al., 2024), with supplementary grain size fractions (Clay, Silt, Sand) projected as a posteriori variables (red vectors). Samples are colored by K-means cluster classification (k = 3) (**B**) Down core variation expressed by different element ratios along with grain size analysis of units 2 to 4. (For interpretation of the references to colour in this figure legend, the reader is referred to the web version of this article.)

plots on the negative side of PC1 and PC2, while Cluster 2 (7.6–14.1 cal kyr BP) and Cluster 3 (14.1–16.9 cal kyr BP) plot along the positive axis of PC1. Grain-size parameters (clay, silt, and sand) were projected post hoc as supplementary variables. These are strongly aligned with PC1, indicating a strong association between sediment texture and geochemical composition. In particular, sand content correlates with SiO_2 and Zr, suggesting a detrital or coarse-grained input, whereas finer fraction (silt) correspond more closely with Al_2O_3, K_2O, and other lithogenic elements.

Log ratios of SiO_2 and Zr against Al_2O_3, CaO, TiO_2, and MgO demonstrate lithogenic variability down the core, particularly between 42 and 50 cm and 155–217 cm (Fig. 3B). Log ratios of Fe_2O_3, MnO, and P_2O_5 with Al_2O_3 exhibit down-core autogenic/biogenic variation, particularly between 0 and 75 cm (Fig. 3B).

4.3. Organic geochemistry

TOC ranges from 0.2 to 14.5 % with an average of 4.5 %. Unit 3 yielded the highest TOC values (av. 9 %), followed by Unit 2 (av. 4 %) and Unit 4 (av. 2.9 %). From bottom to top, TOC values show an increasing trend reaching a maximum at 185 cm depth which also roughly coincides with a layer rich in traces of root material. Values decrease upwards. TOC/N values range from 2.5 to 14 (average of 9.2). The highest ratio roughly coincides with the boundary between Unit 3 and Unit 4 (125 cm). $\delta^{13}C$ values range between −6 and − 16 ‰ (average of −13.2 ‰). In Unit 2, $\delta^{13}C$ values start with a low value and strongly shift towards positive trend reaching a maximum at 325 cm and gradually shift towards depletion trend throughout the core (Fig. 4A).

The sugar contents resemble the trends of TOC and reveal generally high values in Unit 3 (av. 15, 59 and 22 mg g^{-1} for arabinose, fucose, and xylose, respectively) followed by Unit 4 (av. 7, 28 and 11 mg g^{-1} for arabinose, fucose, and xylose, respectively) and Unit 2 (0.2, 2.4 and 1.1

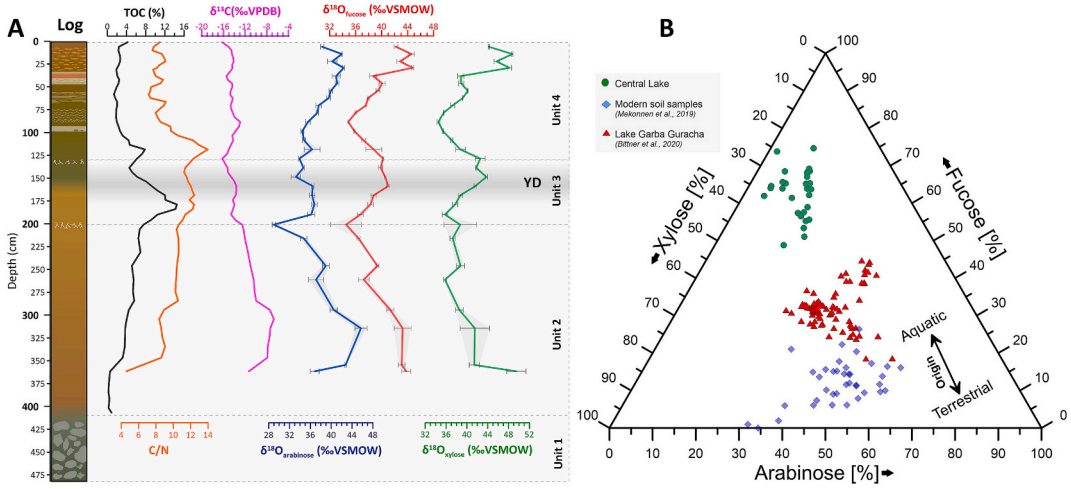

Fig. 4. (**A**) Down core basic organic geochemical characterization (TOC, TOC/N and $\delta^{13}C$) and compound specific $\delta^{18}O$ values for arabinose, fucose and xylose. (**B**) Ternary diagram showing relative distribution of arabinose, fucose and xylose for Central Lake sediment indicators for organic matter source (after Hepp et al., 2016). Sugar biomarker values from Garba Guracha (Bittner et al., 2020) and modern soil samples from the surrounding catchment (Mekonnen et al., 2019) are displayed for comparison.

mg g^{-1} for arabinose, fucose, and xylose, respectively). Molecular ratios $\left(\frac{[Fuc]}{[Ara+Xyl]}\right)$ according to Hepp et al., 2016 are high (well above 0.1) throughout the core with the highest values recorded in Unit 2 (av. 1.9) followed by Unit 4 (1.7) and Unit 3 (1.5) (Table S1).

4.4. $\delta^{18}O$ sugar biomarker record

The $\delta^{18}O$ values range from 29.0 to 49.5 ‰ for all three investigated sugar biomarkers and mostly show similar down core variability (Fig. 4A & Table S2). A significant correlation is observed between fucose and xylose ($R = 0.87$, $p < 0.001$, $n = 29$), followed by fucose and arabinose ($R = 0.65$, $p < 0.001$, $n = 29$). The correlation between xylose and arabinose is below 0.5.

From bottom to top, our Central Lake $\delta^{18}O_{fucose}$ record shows enrichment between 362 and 315 cm (16.2 and 15.5 cal kyr BP) corresponding to the Late Glacial, followed by a gradual depletion trend beginning in Unit 2. The transition from Unit 2 to 3 marks the beginning of a shift towards enrichment again. Unit 3 mainly records enriched $\delta^{18}O$ values. Within dating uncertainties, the strongest ^{18}O enrichment within this unit corresponds with the YD. Unit 4 begins with a depletion trend around 128 cm (10.8 cal kyr BP), coinciding with the African Humid Period (AHP) during the Early to Middle Holocene. The Late Holocene (uppermost 30 cm of Unit 4) shows the strongest enrichment of the record.

5. Discussion

5.1. Sediment provenance, depositional history and lake dynamics

Lithogenic particles primarily originate from the surrounding bedrock based on the following geochemical observations: (i) comparison of sediments with PAAS and UCC reflect the abundance of chemically immature sediment composition (Taylor and McLennan, 1995; Cox et al., 1995; Rudnick and Gao, 2003); (ii) positive correlation between geochemically mobile elements such as K_2O, CaO, Na_2O, TiO_2, MgO with Al_2O3 and TiO_2 indicate common mineralogic origin (likely minerals such as feldspars and olivine which are common in the surrounding bedrock (Nelson et al., 2019)) (iii) Similarity of major and trace element composition with the surrounding volcanic bedrock (Nelson et al., 2019; Table S3).

Calculated element ratios down core (Fig. 3B) generally show low variability, indicating no significant change in sediment provenance. However, between 155 and 185 cm (11.9–13 cal kyr BP, corresponding to YD) and 0-75 cm (< 5 cal kyr BP), we see a shift in the concentration of SiO_2 and Zr (Fig. 3B). Both elements are geochemically less abundant in the surrounding host rocks (Nelson et al., 2019), which may indicate an allochthonous source, likely silica-rich aeolian dust coming from the lowlands (Mekonnen et al., 2022). Modern dust flux studies show deflated fluvial sediments rich in silica from the neighboring lowland regions of the Ogaden basin and the Danakil depression as potential dust sources in the Horn of Africa region (Gherboudj et al., 2017; Kunkelova et al., 2024).

Field observation shows the increasing presence of mottled layers and lateritic laminations, especially the topmost 75 cm layer of unit 4 (Fig. 2). Geochemical results also show a sudden shift in autogenic fractions (Fig. 3B). We interpret this shift as autogenetic/biogenic precipitation of Mn, Fe, and P under emerging conditions in a palustrine setting or seasonal lake desiccation (Föllmi, 1993; Sparrow and Uren, 2014).

5.2. Aquatic versus terrestrial origin of the Central Lake sugar biomarkers

The sugar biomarker ratios (Section 4.3) are well above 0.1 (Hepp et al., 2016) and indicate a predominant aquatic origin of the sugar biomarkers (Table S1). Sugar biomarkers in lacustrine sediments can originate from aquatic (autochthonous) or terrestrial (allochthonous) sources. Fucose often occurs abundantly in aquatic organisms such as phytoplankton, aquatic plants and bacteria, whereas arabinose and xylose are predominant in terrestrial plants (Ogier et al., 2001; Jia et al., 2008; Hepp et al., 2016; Mekonnen et al., 2019, 2023). Moreover, in a ternary diagram, data points from Central Lake and Lake Garba Guracha (Bittner et al., 2022) plot much closer to fucose compared to soil samples from the surrounding catchment (Mekonnen et al., 2019) (Fig. 3B). Distinguishing between these two sources is a prerequisite for robust interpretations of lacustrine $\delta^{18}O$ records (Bittner et al., 2022). The organic matter characteristics further corroborate the predominance of aquatic origin (Fig. 3A). In principle, the observed $\delta^{13}C$ values could indicate C4 vegetation. However, given the absence of evidence for C4 vegetation in the study area (Mekonnen et al., 2019), we prefer to follow the $\delta^{13}C$ interpretation suggested previously by Bittner et al. (2020) for the Garba Guracha sedimentary record in terms of a predominantly aquatic organic matter input. Concerning TOC/N, ratios <10 are often used as an indicator for primarily aquatically produced organic matter

(Meyers, 1994; Strobel et al., 2021), whereas ratios >20 are usually only found in higher terrestrial plants. The Central Lake TOC/N record with mostly ratios <12 is hence well in agreement with the assumption of sedimentary organic matter being mainly of aquatic origin.

5.3. Interpretation of the Central Lake $\delta^{18}O_{fucose}$ record

Since fucose of Central Lake sediments is primarily of aquatic origin, reconstructing $\delta^{18}O$ of lake water using established methods (Zech et al., 2014b; Hepp et al., 2015; Bittner et al., 2022) is feasible. This reconstruction relies on an apparent biosynthetic fractionation factor (ε_{bio}), typically around 29 ‰ for aquatic sugars (Mayr et al., 2015), which is slightly higher than the ~27 ‰ observed for terrestrial cellulose (Hepp et al., 2015; Lehmann et al., 2017). Bittner et al., 2022 confirmed the validity of using $\varepsilon_{bio} = 29$ ‰ by comparing biomarker-derived $\delta^{18}O$ lake water with $\delta^{18}O_{diatoms}$, showing that both reflect lake water isotopic variability driven by the precipitation-to-evaporation (P/E) balance.

In Central Lake, reconstructed $\delta^{18}O_{lakewater}$ values range from +6 ‰ to +16 ‰. For comparison, modern precipitation $\delta^{18}O$ measurements from 2017 at three meteorological stations surrounding Central Lake averaged approximately −4 ‰ (Lemma et al., 2020; Figs. 1 & 5B). Contemporary lake water sample collected from Lake Garba Guracha shows a mean $\delta^{18}O$ value of +4.7 ‰ ± 0.6 ‰ (Bittner et al., 2022). Moreover, Lemma et al. (2021) analyzed $\delta^{18}O$ values from sugar biomarkers in dominant plant species and topsoil samples in the Bale Mountains, finding minimal inter-species variability and no significant degradation of the isotopic signal due to post-depositional processes. Comparing our lake water biomarker $\delta^{18}O$ values with the plant dataset

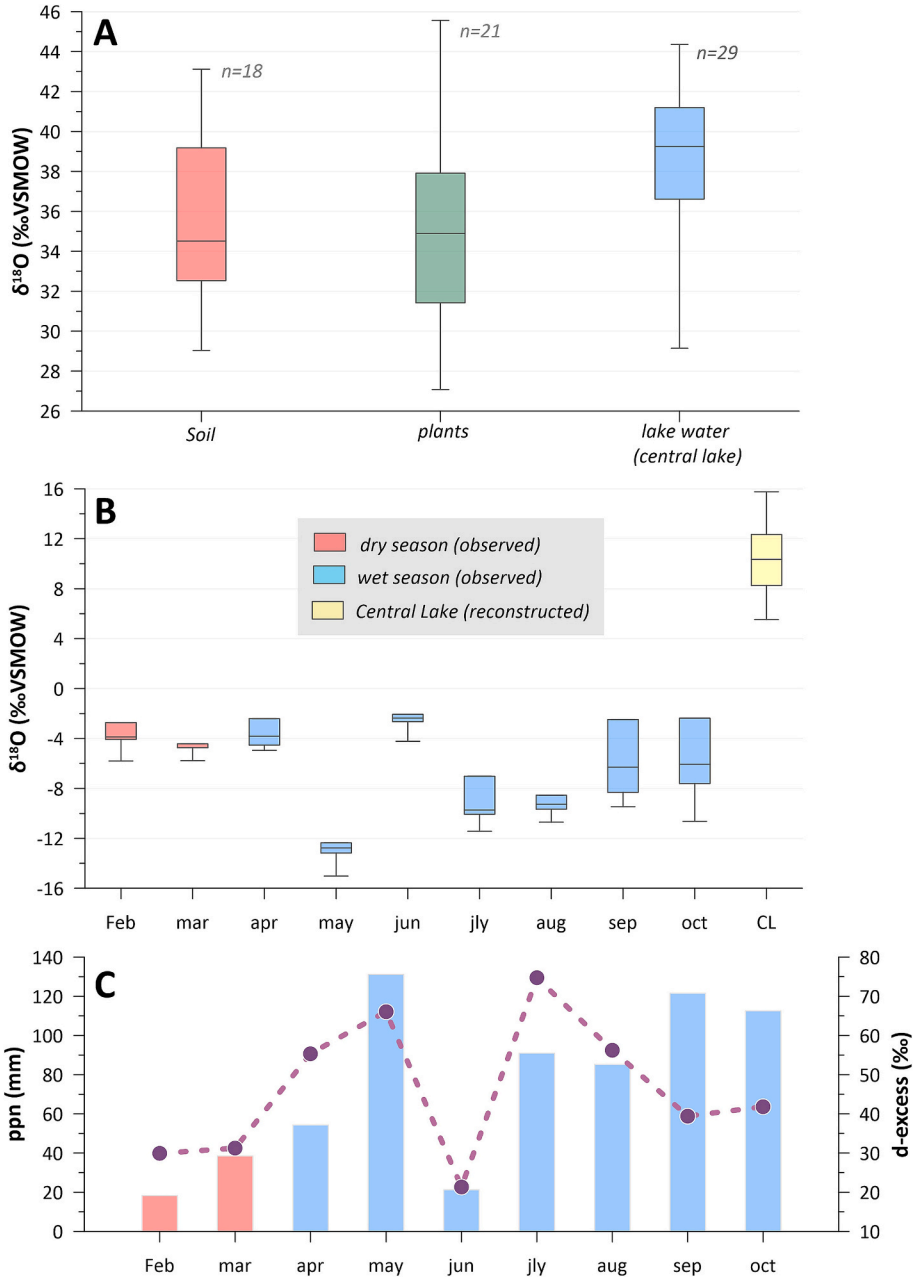

Fig. 5. (**A**) Comparison of $\delta^{18}O_{sugar}$ of Central Lake with modern samples from dominant plant species and soil within an altitudinal range of 3800 to 4300 m a.s.l.) (Lemma et al., 2021). For details of selected plant species and soil samples, readers are referred to the original work. (**B**) Comparison of reconstructed $\delta^{18}O_{lake\ water}$ of Central Lake with modern $\delta^{18}O_{preciptation}$ (Lemma et al., 2020). Data collected from the three weather stations (indicated in Fig. 1) in 2017. (**C**) Modern seasonal precipitation (ppn.) and d-excess (dashed line) patterns for the aforementioned weather stations.

reveals a significant enrichment (Bonferroni-adjusted $p < 0.01$). In contrast, the difference between lake and soil sugar $\delta^{18}O$ values is not statistically significant ($p > 0.05$) (Fig. 5B). These findings support the interpretation that the $\delta^{18}O_{lakewater}$ signal is primarily driven by evaporative enrichment.

When interpreting $\delta^{18}O$ records, several key factors must be considered, including precipitation amount, source region, temperature, altitude gradients, and the extent of moisture recycling (Sharp, 2017). Specifically: (i) In tropical regions, temperature exerts a relatively minor influence on $\delta^{18}O$ variability compared to temperate zones. (ii) Rather, precipitation amount and moisture source are dominant controls on $\delta^{18}O$ in rainfall, especially within the study area (Lemma et al., 2020; Bittner et al., 2022).

It is also important to acknowledge the potential past influence of the isotopically depleted Congo Air Mass (CAM), which has been linked to Holocene $\delta^{18}O$ signals in the archives of Lake Tana and Lake Dendi in the northwestern Ethiopian Highlands (Costa et al., 2014; Jaeschke et al., 2020). Although modern back-trajectory analyses suggest that CAM does not presently contribute moisture to the Bale Mountains (Lemma et al., 2020), its influence in the past cannot be entirely excluded from the study area (Junginger et al., 2014; Bittner et al., 2022). While we currently lack the data to separate CAM contributions quantitatively, it

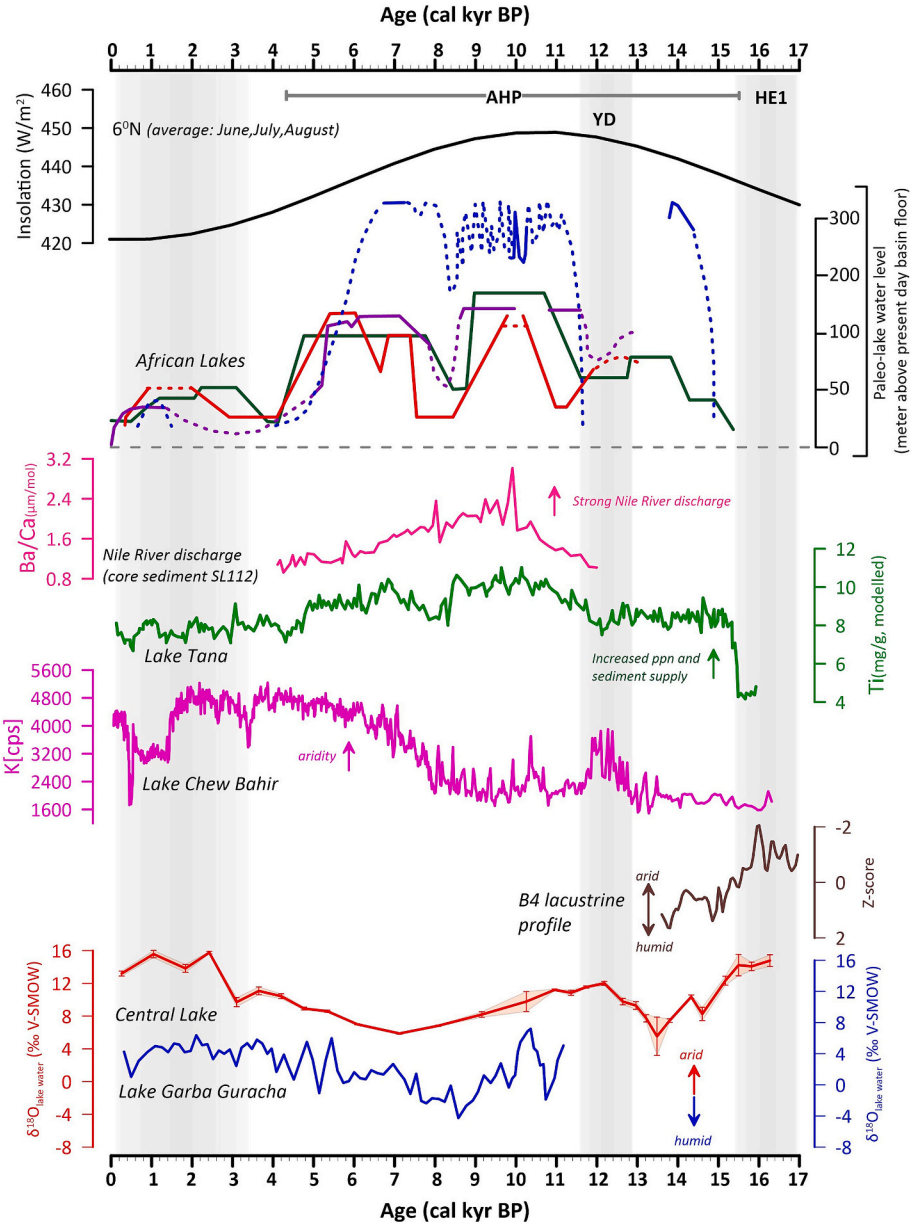

Fig. 6. Comparison of Central Lake record with different hydroclimate archives from East Africa and neighboring regions. $\delta^{18}O_{lake\ water}$ Lake Garba Guracha (Bittner et al., 2022), and Central Lake (this study). 'B4' lacustrine profile (Mekonnen et al., 2022), *Z*-score is calculated form black carbon (BC) and pollen (*Artemisia*/*Chenopodiaceae* (A/C) ratio) proxies; Chew Bahir Potassium (K) record as an aridity index (Foerster et al., 2012); Ti concentration from Lake Tana reflecting detrital input as precipitation increase lake level highstand (Marshall et al., 2011); Ba/Ca ratio extracted from planktonic foraminifera from sediment core SL112 in Levant Basin indicating Nile river discharge strength and associated East African Monsoon (Weldeab et al., 2014); Lake level reconstructions of African Lakes; Ziway-Shala (Gillespie et al., 1983) *red*; Lake Turkana (Garcin et al., 2012) *violate*, paleo-Lake Suguta (Junginger et al., 2014)*blue*,; Lake Bosumtwi (Shanahan et al., 2006) *green*; Northern Hemisphere insolation variation for Bale Mountains region (Laskar et al., 2004). (AHP) African Humid Period, (YD) Younger Dryas and (HE1) Heinrich Event 1. Refer to Fig. 1 for location of the climate archives mentioned here. (For interpretation of the references to colour in this figure legend, the reader is referred to the web version of this article.)

is essential to note that our biomarker proxy reconstructs $\delta^{18}O_{lakewater}$, rather than $\delta^{18}O_{precipitation}$, directly. As such, it remains a robust indicator of past hydroclimatic conditions driven by changes in P/E (Bittner et al., 2022). Accordingly, during wet periods, open lake conditions characterized by inflow and outflow resulted in only minor ^{18}O enrichment of lake water. By contrast, during dry periods, closed lake conditions prevailed resulting in high ^{18}O enrichment (Fig. S1).

5.4. Comparison of the Central Lake $\delta^{18}O_{fucose}$ record with the Garba Guracha $\delta^{18}O_{fucose}$ record

A closer look and comparison of the Central Lake with the Garba Guracha $\delta^{18}O_{fucose}$ record indicate difference in magnitude despite having similar long-term trends (Fig. 5). The reconstructed lake water ranges of +6 to +16 ‰ and − 4.3 to +7.2 ‰ for Central Lake and Garba Guracha (Bittner et al., 2022), respectively (Fig. 6). This difference is likely due to Central Lake's shallow and semi-intermittent nature, whereas Garba Guracha is a perennial lake and maintains a relatively constant water level (4–6 m water depth) throughout the year (Eggermont et al., 2011; Bittner et al., 2020). This disparity results in an unequal evaporation rate in a lake with a smaller catchment area, which may result in an amplified enrichment signal (cf. Skrzypek et al., 2015); during sustained drought events, the lake may quickly dry up and desiccate, potentially diminishing or entirely halting the production of aquatic organic matter. This scenario could result in underestimating the severity of these drought events. In the modern context, the lake experiences change from a shallow lacustrine to a palustrine wetland on a seasonal basis. The mottled layers observed at the top of the core (cf. Unit 4 in Section 4.1) corroborate this. These layers also yielded the most positive $\delta^{18}O$ values in the dataset (Fig. 4A). It is worth noting that Mekonnen et al. (2022) reported two Late Pleistocene desiccation layers and a hiatus (16.3 and 13.6–10.2 cal kyr BP), respectively, for the sediment record called B4 in the northwestern region of the Sanetti Plateau not far away from Central Lake (Fig. 1). The Holocene Unit 3 of B4 well resembles the top most 70 cm of Unit 4 of Central Lake.

Another difference between Central Lake and Garba Guracha is that the Holocene Central Lake $\delta^{18}O_{fucose}$ record seems "smoothed" compared to the Garba Guracha $\delta^{18}O_{fucose}$ record. This might be explained by the Garba Guracha dataset having a ~ 100-year resolution, whereas the Holocene part of Central Lake has a ~ 750-year resolution. Nevertheless, despite this disparity in sampling frequency, the $\delta^{18}O_{fucose}$ values in both datasets exhibit analogous millennial-scale climate variations (Fig. 6).

5.5. Hydroclimatic implications as derived from the Central Lake $\delta^{18}O_{fucose/lake\ water}$ and other records from the region

5.5.1. Late glacial arid phase (16.2 cal kyr BP)

Between 16.2 and 15.5 cal kyr BP, our Central Lake record shows a marked isotopic enrichment of approximately +15 ‰, indicating an endorheic lake phase associated with arid climatic conditions. The desiccation layer, dated to ~16.3 cal kyr BP in the nearby B4 sedimentary sequence (Mekonnen et al., 2022), supports this interpretation. Similarly, Casas-Gallego et al. (2023) documented the dominance of dry Afromontane vegetation across the Ethiopian Highlands during the final millennium of the Last Glacial Maximum (~17 cal kyr BP).

Regionally, synchronous dry phases have been reported, including 16.4–15.9 cal kyr BP at Lake Tana (Marshall et al., 2011); arid conditions persisting beyond 15 cal kyr BP in the Chew Bahir Basin (Foerster et al., 2012, 2015); the development of paleosols around ~15.3 cal kyr BP at Lakes Victoria and Albert (Gasse, 2000; Stager et al., 2002); and drought phase prior to 16.3 cal kyr BP in the Gulf of Guinea and Lake Bosumtwi (Shanahan et al., 2006; Marret et al., 2013).

Although slight chronological discrepancies exist among individual records, the broader picture reveals a widespread weakening of regional hydrological cycles in the aftermath of the Last Glacial Maximum, with arid conditions prevailing across both hemispheres of the African continent (Gasse, 2000; Stager et al., 2011; Otto-Bliesner et al., 2014). Sea surface temperature (SST) reconstructions also indicate cooling in the Arabian Sea and the western Indian Ocean, likely driven by Antarctic-sourced deep-water surges coinciding with Heinrich ice-rafting events in the Atlantic (Jung et al., 2009; Romahn et al., 2014). Climate simulations also demonstrate the key role of these events in weakening the Afro-Asian monsoon system (Tierney et al., 2016).

5.5.2. The onset of AHP (15.5 cal kyr BP or 10.5 cal yr BP?)

At 15 cal kyr BP, our Central Lake $\delta^{18}O$ record shows an abrupt shift towards wetter conditions (Fig. 5). The black carbon (BC) and pollen data from the B4 profile (Mekonnen et al., 2022) reveal increased biomass productivity and fire intensity on the Sanetti Plateau between 15.7 and 14.4 cal kyr BP, coinciding with the onset of the African Humid Period (AHP) in the Bale Mountains (Fig. 5). Umer et al. (2007) reported a rise in pollen influx in Lake Garba Guracha around 13.4 cal kyr BP due to enhanced moisture availability. In contrast, based on the Holocene $\delta^{18}O_{fucose}$ record, Bittner et al. (2022) proposed that the AHP began around 10.5 cal kyr BP in the Bale Mountains. Our findings provide extended $\delta^{18}O_{fucose}$ evidence of the onset of the AHP at approximately 15 cal kyr BP. Gasse (2000) noted that the transition from the Last Glacial Maximum (LGM) to the AHP included two dry-wet transitions at 15–14.5 cal kyr BP and 11.5–11 cal kyr BP. We also observe a brief return to a dry spell between 12.8 and 10.5 cal kyr BP in our $\delta^{18}O$ record, which corresponds to the Younger Dryas (YD) event (Fig. 7). A sudden shift in lithogenic element ratios (Fig. 3B) implies increased dust input under dry conditions. Gil-Romera et al. (2021) also interpreted the abrupt decline of Afro-alpine vegetation in the Lake Garba Guracha pollen record as a resumption of a short and abrupt cold/dry pulse. Thus, we interpret the dry-to-wet transition around 10.5 cal kyr BP observed in both Lake Garba Guracha and Central Lake records (Fig. 7) as the second transition phase of the AHP in the Bale Mountains.

The arid-to-humid transition around 15 cal kyr BP is also observed in the Chew Bahir basin (Foerster et al., 2012, 2015); paleo-Lake Suguta (Junginger et al., 2014); Lake Tana (Marshall et al., 2011); and Lake Tanganyika (Tierney et al., 2008). The second arid-to-humid transition is also recorded in several lake archives (Gillespie et al., 1983; Shanahan et al., 2006; Tierney and Russell, 2007; Foerster et al., 2012; Marret et al., 2013; Junginger et al., 2014).

5.6. Early Holocene humid phase and termination of the AHP (10.5 cal kyr BP to Present)

In the Bale Mountains, humid conditions re-emerged between ~11 and 10.8 cal kyr BP. Proxy records from Lake Garba Guracha (Gil-Romera et al., 2019, 2021; Bittner et al., 2020; Bittner et al., 2022) indicate peak humidity, high ecosystem productivity, and thermal maxima during the interval from ~10.5 to 6 cal kyr BP. The $\delta^{18}O$ record from Central Lake exhibits an overall trend consistent with these observations, albeit with less detailed variability (see Section 5.3 for further discussion).

For example, the well-documented 8.2 cal kyr BP drought event, which is evident in many Eastern African archives (e.g., Gillespie et al., 1983; Gasse, 2000; Thompson et al., 2002; Junginger et al., 2014), is not apparent in our Central Lake record. This absence is also seen in the high-resolution $\delta^{18}O$ record from Lake Garba Guracha (Bittner et al., 2022), which, despite a sampling resolution of 100–250 years, shows no significant isotopic excursion. Similarly, Gil-Romera et al. (2021) reported no marked changes in vegetation communities based on the pollen record during this interval. These findings suggest that, despite our sampling resolution being comparatively lower, the main hydroclimatic signals are still effectively captured.

According to Bittner et al. (2022), centennial-scale variations in the Garba Guracha Holocene record largely reflect increasing influence from the seasonal monsoon system, consistent with broader monsoon

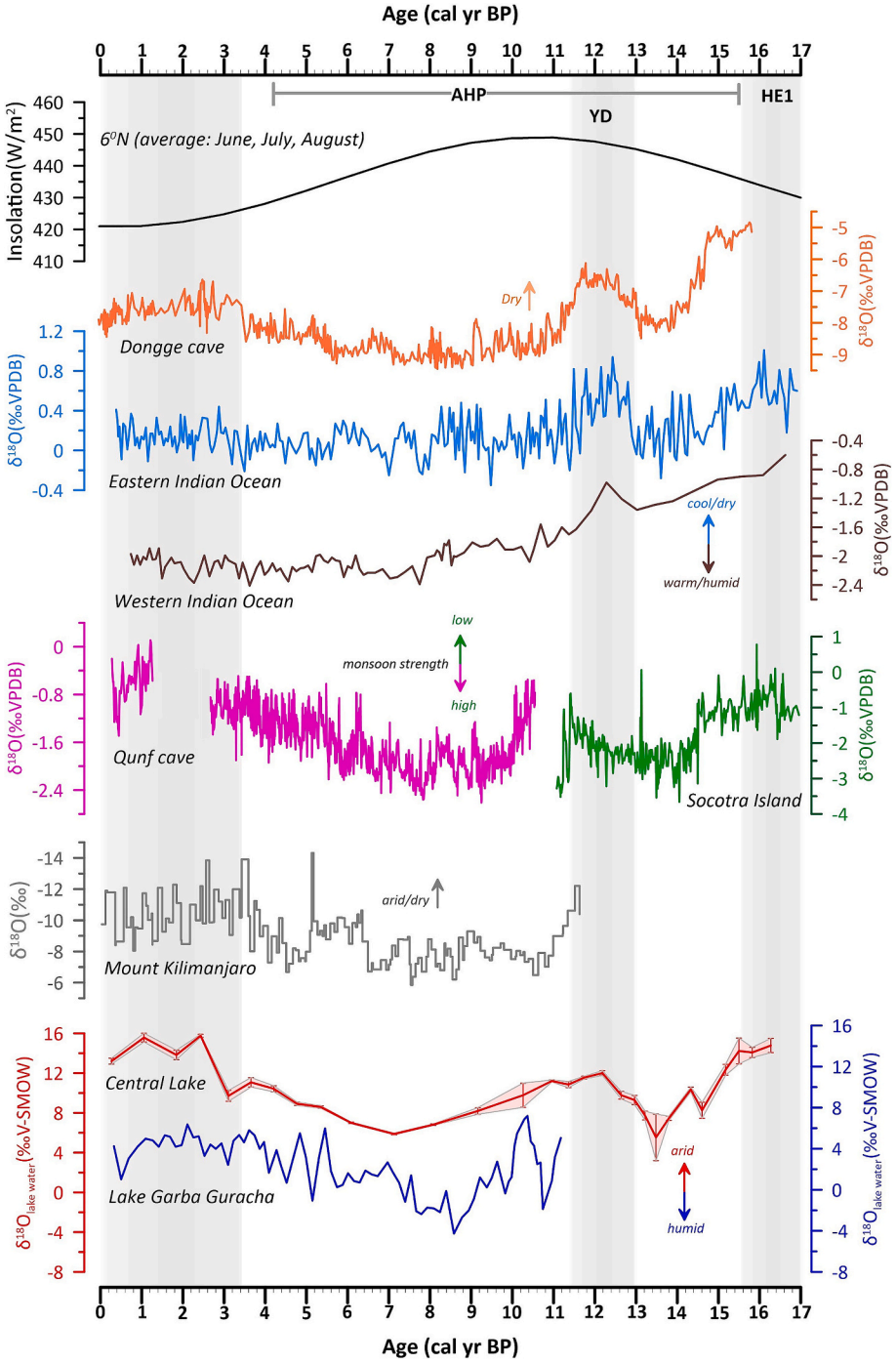

Fig. 7. Comparison of $\delta^{18}O$ records from different archives within the influence of ITCZ. $\delta^{18}O_{lake\ water}$ records from Afro Alpine Bale Mountains (Bittner et al., 2022, this work); 50 year average $\delta^{18}O$ record from Kilimanjaro ice cores (Thompson et al., 2002); $\delta^{18}O$ records from Qunf cave, Yemen (Fleitmann et al., 2003); $\delta^{18}O$ records from Socotra Island, Yemen (Shakun et al., 2007); $\delta^{18}O_{planktic}$ Marine core record GeoB12615–4 (Romahn et al., 2014) from Western Indian Ocean; $\delta^{18}O_{sea\ water}$ record from core 39 KL in Eastern Indian Ocean (Mohtadi et al., 2014); $\delta^{18}O$ records from Dongge caves (Dykoski et al., 2005); Northern Hemisphere insolation variation (Laskar et al., 2004). Refer to Fig. 1 for location of the climate archives mentioned here.

dynamics described in records from Asia and the Middle East (e.g., Fleitmann et al., 2003; Dykoski et al., 2005; Meyer et al., 2020).

After ~6 cal kyr BP, our $\delta^{18}O$ record shows a steady enrichment trend, which, together with changes in geochemical ratios (e.g., increasing SiO_2 and Zr relative to Al_2O_3 and TiO_2; Fig. 3B) suggests intensified dust flux into the region. These geochemical signatures are interpreted as responses to changes in hydroclimate, particularly precipitation-to-evaporation (P/E) balance and vegetation cover. Regionally, this trend aligns with increased dust mobilization observed throughout Eastern Africa (Jung et al., 2004; Weldeab et al., 2014). Jung et al. (2004) reported a gradual rise in dust flux from northeastern Africa, beginning around 6.4 cal kyr BP, which marked a stepwise shift towards the arid landscape of today. This transformation parallels a progressive weakening of the East African Monsoon (EAM), also recorded in declining Nile River runoff (Weldeab et al., 2014).

The most pronounced $\delta^{18}O$ enrichment in Central Lake occurs after ~3.1 cal kyr BP (Figs. 6 & 7). Oxidized and mottled sediment layers indicate increased seasonality and a shift towards palustrine lake

conditions (Fig. 2). Under such conditions, aquatic sugar production may be disrupted by periodic lake desiccation, potentially leading to under- or overestimation of climatic signals. Hence, the $\delta^{18}O$ signal of this horizon represents seasonal lake dynamics rather than regional hydroclimate. Notably, no comparable sedimentological features or anomalously high $\delta^{18}O$ values are observed in the Lake Garba Guracha record (Bittner et al., 2020; Bittner et al., 2022), further supporting our interpretation of increasing seasonality and aridity in Central Lake during the Late Holocene.

6. Conclusions

The sediments of Central Lake represent a valuable archive of the Late Glacial-Holocene paleoenvironmental history of Africa's largest alpine ecosystem. It thus allows complementing the Holocene and Late Glacial, but incomplete, records of the neighboring Garba Guracha and B4 sedimentary archives. The investigated sugar biomarkers are characterized by the dominance of fucose, which is a strong indication of primarily aquatic production. We established a $\delta^{18}O_{sugar}$ record by applying compound-specific $\delta^{18}O$ analysis. The $\delta^{18}O_{fucose/lake\ water}$ record of Central Lake and the neighboring Lake Garba Guracha (Bittner et al., 2022) primarily reflect precipitation to evaporation (P/E) changes. Geochemical ratios also indicate periodic dust input during dry phases, particularly corresponding to the Younger Dryas (YD) and Late Holocene periods, along with intensified seasonal lake desiccation. The concurrence of shifts in Central Lake proxies with significant climatic events, such as the African Humid Period (AHP) and the Younger Dryas (YD), across various microclimatic environments in the region indicates a notable climatic teleconnection.

CRediT authorship contribution statement

Samuel G. Chernet: Writing – original draft, Methodology, Formal analysis, Conceptualization. **Lucas Bittner:** Formal analysis, Data curation, Conceptualization. **Graciela Gil-Romera:** Resources, Project administration, Data curation, Conceptualization. **Bruk Lemma:** Investigation, Writing – review & editing. **Marcel Bliedtner:** Formal analysis. **Roland Zech:** Resources, Formal analysis. **Bruno Glaser:** Resources, Formal analysis. **Tobias Bromm:** Formal analysis. **Sönke Szidat:** Formal analysis. **Wolfgang Zech:** Project administration, Data curation. **Michael Zech:** Supervision, Funding acquisition, Data curation, Conceptualization.

Declaration of competing interest

The authors declare the following financial interests/personal relationships which may be considered as potential competing interests:

Michael Zech reports financial support was provided by German Research Foundation. If there are other authors, they declare that they have no known competing financial interests or personal relationships that could have appeared to influence the work reported in this paper.

Acknowledgments

This project was funded by German Research Foundation (DFG, ZE 844/14-1 and ZE 844/21-1). We are grateful to the Addis Ababa University, the Bale Mountains National Park, and the Ethiopian Wildlife Conservation Authority for their support during field work and scientific collaboration. Katinka Thielsen, Betelhem Mekonnen and Mekbib Fekadu are duly acknowledged for their support during field campaign. SGC especially thanks the team members of the Biomarker Laboratory at TU-Dresden, namely Marika Stutzriemer, Carsten Marburg, Annika Weigel and Fabian Seemann for their support during laboratory analysis.

Appendix A. Supplementary data

Supplementary data to this article can be found online at https://doi.org/10.1016/j.gloplacha.2025.104975.

Data availability

The authors confirm that all data necessary for supporting the scientific findings of this paper have been provided.

References

Amelung, W., Cheshire, M.V., Guggenberger, G., 1996. Determination of neutral and acidic sugars in soil by capillary gas-liquid chromatography after trifluoroacetic acid hydrolysis. Soil Biol. Biochem. 28, 1631–1639. https://doi.org/10.1016/S0038-0717(96)00248-9.

Baker, A., Asrat, A., Fairchild, I.J., Leng, M.J., Wynn, P.M., Bryant, C., Genty, D., Umer, M., 2007. Analysis of the climate signal contained within $\delta^{18}O$ and growth rate parameters in two Ethiopian stalagmites. Geochim. Cosmochim. Acta 71, 2975–2988. https://doi.org/10.1016/J.GCA.2007.03.029.

Benettin, P., Volkmann, T.H.M., Freyberg, J.V., Frentress, J., Penna, D., Dawson, T.E., Kirchner, J.W., 2018. Effects of climatic seasonality on the isotopic composition of evaporating soil waters. Hydrol. Earth Syst. Sci. 22, 2881–2890. https://doi.org/10.5194/HESS-22-2881-2018.

Bertrand, S., Tjallingii, R., Kylander, M.E., Wilhelm, B., Roberts, S.J., Arnaud, F., Brown, E., Bindler, R., 2024. Inorganic geochemistry of lake sediments: a review of analytical techniques and guidelines for data interpretation. Earth Sci. Rev. 249, 104639. https://doi.org/10.1016/J.EARSCIREV.2023.104639.

Bittner, L., Bliedtner, M., Grady, D., Gil-Romera, G., Martin-Jones, C., Lemma, B., Mekonnen, B., Lamb, H.F., Yang, H., Glaser, B., Szidat, S., Salazar, G., Rose, N.L., Opgenoorth, L., Miehe, G., Zech, W., Zech, M., 2020. Revisiting Afro-alpine Lake Garba Guracha in the Bale Mountains of Ethiopia: rationale, chronology, geochemistry, and paleoenvironmental implications. J. Paleolimnol. 64, 293–314. https://doi.org/10.1007/s10933-020-00138-w.

Bittner, L., Gil-Romera, G., Grady, D., Lamb, H.F., Lorenz, E., Weiner, M., Meyer, H., Bromm, T., Glaser, B., Zech, M., Wegener, A., 2022. The Holocene lake-evaporation history of the Afro-alpine Lake Garba Guracha in the Bale Mountains, Ethiopia, based on $\delta^{18}O$ records of sugar biomarker and diatoms. https://doi.org/10.1017/qua.2021.26.

Blaauw, M., Christen, J.A., 2011. Flexible paleoclimate age-depth models using an autoregressive gamma process. Bayesian Anal. 6, 457–474. https://doi.org/10.1214/11-BA618.

Camberlin, P., 1997. Rainfall anomalies in the source region of the Nile and their connection with the Indian Summer Monsoon. J. Climate 10, 1380–1392. https://doi.org/10.1175/1520-0442(1997)010<1380:RAITSR>2.0.CO;2.

Casas-Gallego, M., Hahn, K., Neumann, K., Demissew, S., Schmidt, M., Bodin, S.C., Bruch, A.A., 2023. Cooling-induced expansions of Afromontane forests in the Horn of Africa since the Last Glacial Maximum. Sci. Rep. 13, 1–10. https://doi.org/10.1038/s41598-023-37135-8.

Castañeda, I.S., Schouten, S., Pätzold, J., Lucassen, F., Kasemann, S., Kuhlmann, H., Schefuß, E., 2016. Hydroclimate variability in the Nile River Basin during the past 28,000 years. Earth Planet. Sci. Lett. 438, 47–56. https://doi.org/10.1016/J.EPSL.2015.12.014.

Costa, K., Russell, J., Konecky, B., Lamb, H., 2014. Isotopic reconstruction of the African Humid Period and Congo Air Boundary migration at Lake Tana, Ethiopia. Q. Sci. Rev. 83, 58–67. https://doi.org/10.1016/J.QUASCIREV.2013.10.031.

Cox, R., Lowe, D.R., Cullers, R.L., 1995. The influence of sediment recycling and basement composition on evolution of mudrock chemistry in the southwestern United States. Geochim. Cosmochim. Acta 59, 2919–2940. https://doi.org/10.1016/0016-7037(95)00185-9.

Duan, D., Zhang, D., Yang, Y., Wang, J., Chen, J., Ran, Y., 2017. Source, composition, and environmental implication of neutral carbohydrates in sediment cores of subtropical reservoirs, South China. Biogeosciences 14, 4009–4022. https://doi.org/10.5194/BG-14-4009-2017.

Dykoski, C.A., Edwards, R.L., Cheng, H., Yuan, D., Cai, Y., Zhang, M., Lin, Y., Qing, J., An, Z., Revenaugh, J., 2005. A high-resolution, absolute-dated Holocene and deglacial Asian monsoon record from Dongge Cave, China. Earth Planet. Sci. Lett. 233, 71–86. https://doi.org/10.1016/J.EPSL.2005.01.036.

Eggermont, H., Wondafrash, M., Van Damme, M., Lens, K., Umer, M.H., 2011. Bale Mountains lakes: ecosystems under pressure of global change? Walia 2011, 171–180.

Fleitmann, D., Burns, S.J., Mudelsee, M., Neff, U., Kramers, J., Mangini, A., Matter, A., 2003. Holocene forcing of the Indian monsoon recorded in a stalagmite from Southern Oman. Science 300, 1737–1739. https://doi.org/10.1126/science.1083130.

Foerster, V., Junginger, A., Langkamp, O., Gebru, T., Asrat, A., Umer, M., Lamb, H.F., Wennrich, V., Rethemeyer, J., Nowaczyk, N., Trauth, M.H., Schaebitz, F., 2012. Climatic change recorded in the sediments of the Chew Bahir basin, southern Ethiopia, during the last 45,000 years. Quat. Int. 274, 25–37. https://doi.org/10.1016/J.QUAINT.2012.06.028.

Foerster, V., Vogelsang, R., Junginger, A., Asrat, A., Lamb, H.F., Schaebitz, F., Trauth, M. H., 2015. Environmental change and human occupation of southern Ethiopia and

northern Kenya during the last 20,000 years. Quat. Sci. Rev. 129, 333–340. https://doi.org/10.1016/J.QUASCIREV.2015.10.026.
Föllmi, K.B., 1993. Phosphorus and phosphate-rich sediments, an environmental approach. Chem. Geol. 107, 375–378. https://doi.org/10.1016/0009-2541(93)90213-3.
Friis, I., 1986. Zonation of forest vegetation on the south slope of Bale Mountains, South Ethiopia. Sinet 9, 29–44.
Garcin, Y., Melnick, D., Strecker, M.R., Olago, D., Tiercelin, J.J., 2012. East African mid-Holocene wet–dry transition recorded in palaeo-shorelines of Lake Turkana, northern Kenya Rift. Earth Planet. Sci. Lett. 331–332, 322–334. https://doi.org/10.1016/J.EPSL.2012.03.016.
Gasse, F., 2000. Hydrological changes in the African tropics since the Last Glacial Maximum. Quat. Sci. Rev. 19, 189–211. https://doi.org/10.1016/S0277-3791(99)00061-X.
Gherboudj, I., Beegum, S.N., Ghedira, H., 2017. Identifying natural dust source regions over the Middle-East and North-Africa: estimation of dust emission potential. Earth Sci. Rev. 165, 342–355. https://doi.org/10.1016/j.earscirev.2016.12.010.
Gillespie, R., Street-perrott, F.A., Switsur, R., 1983. Post-glacial arid episodes in Ethiopia have implications for climate prediction. Nature 306, 680–683. https://doi.org/10.1038/306680a0.
Gil-Romera, G., Adolf, C., Benito, B.M., Bittner, L., Johansson, M.U., Grady, D.A., Lamb, H.F., Lemma, B., Fekadu, M., Glaser, B., Mekonnen, B., Sevilla-Callejo, M., Zech, M., Zech, W., Miehe, G., 2019. Long-term fire resilience of the Ericaceous Belt, Bale Mountains, Ethiopia. Biol. Lett. 15. https://doi.org/10.1098/rsbl.2019.0357.
Gil-Romera, G., Fekadu, M., Opgenoorth, L., Grady, D., Lamb, H.F., Bittner, L., Zech, M., Miehe, G., 2021. The new Garba Guracha palynological sequence: revision and data expansion. In: Quaternary Vegetation Dynamics – The African Pollen Database, pp. 127–134. https://doi.org/10.1201/9781003162766-9.
Groos, A.R., Akçar, N., Yesilyurt, S., Miehe, G., Vockenhuber, C., Veit, H., 2021. Nonuniform late pleistocene glacier fluctuations in tropical Eastern Africa. Sci. Adv. 7, 6826–6838. https://doi.org/10.1126/sciadv.abb6826.
Hepp, J., Tuthorn, M., Zech, R., Mügler, I., Schlütz, F., Zech, W., Zech, M., 2015. Reconstructing lake evaporation history and the isotopic composition of precipitation by a coupled δ18O–δ2H biomarker approach. J. Hydrol. 529, 622–631. https://doi.org/10.1016/J.JHYDROL.2014.10.012.
Hepp, J., Rabus, M., Anhäuser, T., Bromm, T., Laforsch, C., Sirocko, F., Glaser, B., Zech, M., 2016. A sugar biomarker proxy for assessing terrestrial versus aquatic sedimentary input. Org. Geochem. 98, 98–104. https://doi.org/10.1016/J.ORGGEOCHEM.2016.05.012.
Hepp, J., Mayr, C., Rozanski, K., Schäfer, I.K., Tuthorn, M., Glaser, B., Juchelka, D., Stichler, W., Zech, R., Zech, M., 2021. Validation of a coupled δ2Hn-alkane-δ18Osugarpaleohygrometer approach based on a climate chamber experiment. Biogeosciences 18, 5363–5380. https://doi.org/10.5194/BG-18-5363-2021.
Holtvoeth, J., Whiteside, J.H., Engels, S., Freitas, F.S., Grice, K., Greenwood, P., Johnson, S., Kendall, I., Lengger, S.K., Lücke, A., Mayr, C., Naafs, B.D.A., Rohrssen, M., Sepúlveda, J., 2019. The paleolimnologist's guide to compound-specific stable isotope analysis – an introduction to principles and applications of CSIA for Quaternary lake sediments. Quat. Sci. Rev. 207, 101–133. https://doi.org/10.1016/J.QUASCIREV.2019.01.001.
Jaeschke, A., Thienemann, M., Schefuß, E., Urban, J., Schäbitz, F., Wagner, B., Rethemeyer, J., 2020. Holocene hydroclimate variability and vegetation response in the Ethiopian Highlands (Lake Dendi). Front. Earth Sci. 8, 585770. https://doi.org/10.3389/FEART.2020.585770.
Jia, G., Dungait, J.A.J., Bingham, E.M., Valiranta, M., Korhola, A., Evershed, R.P., 2008. Neutral monosaccharides as biomarker proxies for bog-forming plants for application to palaeovegetation reconstruction in ombrotrophic peat deposits. Org. Geochem. 39, 1790–1799. https://doi.org/10.1016/J.ORGGEOCHEM.2008.07.002.
Jung, S.J.A., Davies, G.R., Ganssen, G.M., Kroon, D., 2004. Stepwise Holocene aridification in NE Africa deduced from dust-borne radiogenic isotope records. Earth Planet. Sci. Lett. 221, 27–37. https://doi.org/10.1016/S0012-821X(04)00095-0.
Jung, S.J.A., Kroon, D., Ganssen, G., Peeters, F., Ganeshram, R., 2009. Enhanced Arabian Sea intermediate water flow during glacial North Atlantic cold phases. Earth Planet. Sci. Lett. 280, 220–228. https://doi.org/10.1016/J.EPSL.2009.01.037.
Junginger, A., Roller, S., Olaka, L.A., Trauth, M.H., 2014. The effects of solar irradiation changes on the migration of the Congo Air Boundary and water levels of paleo-Lake Suguta, Northern Kenya Rift, during the African Humid Period (15–5 ka BP). Palaeogeogr. Palaeoclimatol. Palaeoecol. 396, 1–16. https://doi.org/10.1016/J.PALAEO.2013.12.007.
Kebede, S., Travi, Y., 2012. Origin of the δ18O and δ2H composition of meteoric waters in Ethiopia. Quat. Int. 257, 4–12. https://doi.org/10.1016/J.QUAINT.2011.09.032.
Kidane, Y., Stahlmann, R., Beierkuhnlein, C., 2012. Vegetation dynamics, and land use and land cover change in the Bale Mountains, Ethiopia. Environ. Monit. Assess. 184, 7473–7489. https://doi.org/10.1007/s10661-011-2514-8.
Kunkelova, T., Crocker, A.J., Wilson, P.A., Schepanski, K., 2024. Dust source activation frequency in the horn of Africa. J. Geophys. Res. Atmos. 129, e2023JD039694. https://doi.org/10.1029/2023JD039694.
Lamb, H.F., Bates, C.R., Bryant, C.L., Davies, S.J., Huws, D.G., Marshall, M.H., Roberts, H.M., 2018. Author Correction: 150,000-year palaeoclimate record from northern Ethiopia supports early, multiple dispersals of modern humans from Africa. Sci. Rep. 8, 17993. https://doi.org/10.1038/s41598-018-37595-3.
Laskar, J., Robutel, P., Joutel, F., Gastineau, M., Correia, A.C.M., Levrard, B., 2004. A long-term numerical solution for the insolation quantities of the Earth. Astron. Astrophys. 428, 261–285. https://doi.org/10.1051/0004-6361:20041335.
Lehmann, M.M., Gamarra, B., Kahmen, A., Siegwolf, R.T.W., Saurer, M., 2017. Oxygen isotope fractionations across individual leaf carbohydrates in grass and tree species. Plant Cell Environ. 40, 1658–1670. https://doi.org/10.1111/pce.12974.
Lemma, B., Grehl, C., Zech, M., Mekonnen, B., Zech, W., Nemomissa, S., Bekele, T., Glaser, B., 2019. Phenolic compounds as unambiguous chemical markers for the identification of keystone plant species in the Bale Mountains, Ethiopia. Plants 8. https://doi.org/10.3390/plants8070228. Page 228 8, 228.
Lemma, B., Gurmessa, S.K., Nemomissa, S., Otte, I., Glaser, B., Zech, M., 2020. Spatial and temporal 2H and 18O isotope variation of contemporary precipitation in the Bale Mountains, Ethiopia. Isotopes Environ. Health Stud. 56, 122–135. https://doi.org/10.1080/10256016.2020.1717487.
Lemma, B., Bittner, L., Glaser, B., Kebede, S., Nemomissa, S., Zech, W., Zech, M., 2021. δ2Hn-alkane and δ18Osugar biomarker proxies from leaves and topsoils of the Bale Mountains, Ethiopia, and implications for paleoclimate reconstructions. Biogeochemistry 153, 135–153. https://doi.org/10.1007/s10533-021-00773-z.
Liu, X., Rendle-Bühring, R., Henrich, R., 2018. High-and low-latitude forcing of the East African climate since the LGM: inferred from the elemental composition of marine sediments off Tanzania. Quat. Sci. Rev. 196, 124–136. https://doi.org/10.1016/J.QUASCIREV.2018.08.004.
Marret, F., Kim, S.Y., Scourse, J., 2013. A 30,000 yr record of land-ocean interaction in the eastern gulf of Guinea. Quatern. Res. 80, 1–8. https://doi.org/10.1016/J.YQRES.2013.04.003.
Marshall, M.H., Lamb, H.F., Huws, D., Davies, S.J., Bates, R., Bloemendal, J., Boyle, J., Leng, M.J., Umer, M., Bryant, C., 2011. Late Pleistocene and Holocene drought events at Lake Tana, the source of the Blue Nile. Global Planet. Change 78, 147–161. https://doi.org/10.1016/J.GLOPLACHA.2011.06.004.
Mayr, C., Laprida, C., Lücke, A., Martín, R.S., Massaferro, J., Ramón-Mercau, J., Wissel, H., 2015. Oxygen isotope ratios of chironomids, aquatic macrophytes and ostracods for lake-water isotopic reconstructions – results of a calibration study in Patagonia. J. Hydrol. 529, 600–607. https://doi.org/10.1016/J.JHYDROL.2014.11.001.
Mekonnen, B., Zech, W., Glaser, B., Lemma, B., Bromm, T., Nemomissa, S., Bekele, T., Zech, M., 2019. Chemotaxonomic patterns of vegetation and soils along altitudinal transects of the Bale Mountains, Ethiopia, and implications for paleovegetation reconstructions - part 1: stable isotopes and sugar biomarkers. E G Quat. Sci. J. 68, 177–188. https://doi.org/10.5194/EGQSJ-68-177-2019.
Mekonnen, B., Glaser, B., Zech, R., Zech, M., Schlütz, F., Bussert, R., Addis, A., Gil-Romera, G., Nemomissa, S., Bekele, T., Bittner, L., Solomon, D., Manhart, A., Zech, W., 2022. Climate, vegetation and fire history during the past 18,000 years, recorded in high altitude lacustrine sediments on the Sanetti Plateau, Bale Mountains (Ethiopia). Prog. Earth Planet Sci. 9, 14. https://doi.org/10.1186/s40645-022-00472-9.
Mekonnen, B., Bittner, L., Bromm, T., Lemma, B., Glaser, B., Zech, W., Nemomissa, S., Bekele, T., Zech, M., 2023. Terrestrial versus aquatic source identification of sedimentary n-alkane and sugar biomarkers: a case study from the Bale Mountains, Ethiopia. J. Paleolimnol. 70, 347–360. https://doi.org/10.1007/s10933-023-00298-5.
Meyer, I., Daele, M.V., Tanghe, N., Batist, M.D., Verschuren, D., 2020. Reconstructing East African monsoon variability from grain-size distributions: end-member modeling and source attribution of diatom-rich sediments from Lake Chala. Quat. Sci. Rev. 247, 106574. https://doi.org/10.1016/J.QUASCIREV.2020.106574.
Meyers, P.A., 1994. Preservation of elemental and isotopic source identification of sedimentary organic matter. Chem. Geol. 114, 289–302. https://doi.org/10.1016/0009-2541(94)90059-0.
Miehe, S., Miehe, G., 1994. Ericaceous Forest and Heath Land in Bale Mountains of South Ethiopia: Ecology and Man's Impact. Stiftung Walderhaltung, Hamburg (in Afrika).
Mohtadi, M., Prange, M., Oppo, D.W., Pol-Holz, R.D., Merkel, U., Zhang, X., Steinke, S., Lückge, A., 2014. North Atlantic forcing of tropical Indian Ocean climate. Nature 508, 76–80. https://doi.org/10.1038/nature13196.
Nelson, W.R., Hanan, B.B., Graham, D.W., Shirey, S.B., Yirgu, G., Ayalew, D., Furman, T., 2019. Distinguishing plume and metasomatized lithospheric mantle contributions to post-flood basalt volcanism on the southeastern Ethiopian Plateau. J. Petrol. 60, 1063–1094. https://doi.org/10.1093/petrology/egz024.
Nicholson, S.E., 2000. The nature of rainfall variability over Africa on time scales of decades to millenia. Global Planet. Change 26, 137–158. https://doi.org/10.1016/S0921-8181(00)00040-0.
Ogier, S., Disnar, J.R., Albéric, P., Bourdier, G., 2001. Neutral carbohydrate geochemistry of particulate material (trap and core sediments) in an eutrophic lake (Aydat, France). Org. Geochem. 32, 151–162. https://doi.org/10.1016/S0146-6380(00)00138-8.
Osmaston, H.A., Mitchell, W.A., Osmaston, J.A.N., 2005. Quaternary glaciation of the Bale Mountains, Ethiopia. J. Quat. Sci. 20, 593–606. https://doi.org/10.1002/JQS.931.
Otto-Bliesner, B.L., Russell, J.M., Clark, P.U., Liu, Z., Overpeck, J.T., Konecky, B., Demenocal, P., Nicholson, S.E., He, F., Lu, Z., 2014. Coherent changes of southeastern equatorial and northern African rainfall during the last deglaciation. Science 346, 1223–1227. https://doi.org/10.1126/SCIENCE.1259531.
Reimer, P.J., Austin, W.E.N., Bard, E., Bayliss, A., Blackwell, P.G., Ramsey, C.B., Butzin, M., Cheng, H., Edwards, R.L., Friedrich, M., Grootes, P.M., Guilderson, T.P., Hajdas, I., Heaton, T.J., Hogg, A.G., Hughen, K.A., Kromer, B., Manning, S.W., Muscheler, R., Palmer, J.G., Pearson, C., Plicht, J.V.D., Reimer, R.W., Richards, D.A., Scott, E.M., Southon, J.R., Turney, C.S.M., Wacker, L., Adolphi, F., Büntgen, U., Capano, M., Fahrni, S.M., Fogtmann-Schulz, A., Friedrich, R., Köhler, P., Kudsk, S., Miyake, F., Olsen, J., Reinig, F., Sakamoto, M., Sookdeo, A., Talamo, S., 2020. The IntCal20 northern hemisphere radiocarbon age calibration curve (0–55 cal kBP). Radiocarbon 62, 725–757. https://doi.org/10.1017/RDC.2020.41.
Romahn, S., MacKensen, A., Groeneveld, J., Pätzold, J., 2014. Deglacial intermediate water reorganization: new evidence from the Indian Ocean. Clim. Past 10, 293–303. https://doi.org/10.5194/CP-10-293-2014.

Rudnick, R.L., Gao, S., 2003. Composition of the continental crust. Treat. Geochem. 3–9, 1–64. https://doi.org/10.1016/B0-08-043751-6/03016-4.
Schaebitz, F., Asrat, A., Lamb, H.F., Cohen, A.S., Foerster, V., Duesing, W., Kaboth-Bahr, S., Opitz, S., Viehberg, F.A., Vogelsang, R., Dean, J., Leng, M.J., Junginger, A., Ramsey, C.B., Chapot, M.S., Deino, A., Lane, C.S., Roberts, H.M., Vidal, C., Tiedemann, R., Trauth, M.H., 2021. Hydroclimate changes in eastern Africa over the past 200,000 years may have influenced early human dispersal. Commun. Earth Environ. 2, 1–10. https://doi.org/10.1038/s43247-021-00195-7.
Seleshi, Y., Zanke, U., 2004. Recent changes in rainfall and rainy days in Ethiopia. Int. J. Climatol. 24, 973–983. https://doi.org/10.1002/JOC.1052.
Shakun, J.D., Burns, S.J., Fleitmann, D., Kramers, J., Matter, A., Al-Subary, A., 2007. A high-resolution, absolute-dated deglacial speleothem record of Indian Ocean climate from Socotra Island, Yemen. Earth Planet. Sci. Lett. 259, 442–456. https://doi.org/10.1016/J.EPSL.2007.05.004.
Shanahan, T.M., Overpeck, J.T., Wheeler, C.W., Beck, J.W., Pigati, J.S., Talbot, M.R., Scholz, C.A., Peck, J., King, J.W., 2006. Paleoclimatic variations in West Africa from a record of late Pleistocene and Holocene Lake level stands of Lake Bosumtwi, Ghana. Palaeogeogr. Palaeoclimatol. Palaeoecol. 242, 287–302. https://doi.org/10.1016/J.PALAEO.2006.06.007.
Sharp, Z., 2017. Principles of Stable Isotope Geochemistry, 2nd edition. Open Textbooks. https://doi.org/10.25844/h9q1-0p82.
Skrzypek, G., Mydłowski, A., Dogramaci, S., Hedley, P., Gibson, J.J., Grierson, P.F., 2015. Estimation of evaporative loss based on the stable isotope composition of water using hydrocalculator. J. Hydrol. 523, 781–789. https://doi.org/10.1016/J.JHYDROL.2015.02.010.
Sparrow, L.A., Uren, N.C., 2014. Manganese oxidation and reduction in soils: effects of temperature, water potential, pH and their interactions. Soil Res. 52, 483–494. https://doi.org/10.1071/SR13159.
Stager, J.C., Mayewski, P.A., Meeker, L.D., 2002. Cooling cycles, Heinrich event 1, and the desiccation of Lake Victoria. Palaeogeogr. Palaeoclimatol. Palaeoecol. 183, 169–178. https://doi.org/10.1016/S0031-0182(01)00468-0.
Stager, J.C., Ryves, D.B., Chase, B.M., Pausata, F.S.R., 2011. Catastrophic drought in the Afro-Asian monsoon region during Heinrich event 1. Science 331, 1299–1302. https://doi.org/10.1126/SCIENCE.1198322.
Stojanovic, M., Mulualem, G.M., Sorí, R., Vázquez, M., Nieto, R., Gimeno, L., 2022. Precipitation moisture sources of Ethiopian River Basins and their role during drought conditions. Front. Earth Sci. 10, 929497. https://doi.org/10.3389/FEART.2022.929497.
Strobel, P., Struck, J., Zech, R., Bliedtner, M., 2021. The spatial distribution of sedimentary compounds and their environmental implications in surface sediments of Lake Khar Nuur (Mongolian Altai). Earth Surf. Process. Landf. 46, 611–625. https://doi.org/10.1002/ESP.5049.
Strobel, P., Bliedtner, M., Carr, A.S., Struck, J., du Plessis, N., Glaser, B., Meadows, M.E., Quick, L.J., Zech, M., Zech, R., Haberzettl, T., 2022. Reconstructing Late Quaternary precipitation and its source on the southern Cape coast of South Africa: a multi-proxy paleoenvironmental record from Vankervelsvlei. Quat. Sci. Rev. 284, 107467. https://doi.org/10.1016/J.QUASCIREV.2022.107467.
Szidat, S., Salazar, G.A., Vogel, E., Battaglia, M., Wacker, L., Synal, H.-A., Türler, A., 2014. 14C analysis and sample preparation at the new Bern Laboratory for the Analysis of Radiocarbon with AMS (LARA). Radiocarbon 56, 561–566. https://doi.org/10.2458/56.17457.
Taylor, S.R., McLennan, S.M., 1995. The geochemical evolution of the continental crust. Rev. Geophys. 33, 241–265. https://doi.org/10.1029/95RG00262.
Thompson, L.G., Mosley-Thompson, E., Davis, M.E., Henderson, K.A., Brecher, H.H., Zagorodnov, V.S., Mashiotta, T.A., Lin, P.N., Mikhalenko, V.N., Hardy, D.R., Beer, J., 2002. Kilimanjaro ice core records: evidence of holocene climate change in tropical Africa. Science 298, 589–593. https://doi.org/10.1126/SCIENCE.1073198.
Tiercelin, J.J., Gibert, E., Umer, M., Bonnefille, R., Disnar, J.R., Lézine, A.M., Hureau-Mazaudier, D., Travi, Y., Keravis, D., Lamb, H.F., 2008. High-resolution sedimentary record of the last deglaciation from a high-altitude lake in Ethiopia. Quat. Sci. Rev. 27, 449–467. https://doi.org/10.1016/J.QUASCIREV.2007.11.002.
Tierney, J.E., Russell, J.M., 2007. Abrupt climate change in southeast tropical Africa influenced by Indian monsoon variability and ITCZ migration. Geophys. Res. Lett. 34. https://doi.org/10.1029/2007GL029508.
Tierney, J.E., Russell, J.M., Huang, Y., Damsté, J.S.S., Hopmans, E.C., Cohen, A.S., 2008. Northern hemisphere controls on tropical southeast African climate during the past 60,000 years. Science 322, 252–255. https://doi.org/10.1126/science.1160485.
Tierney, J.E., Pausata, F.S.R., Demenocal, P., 2016. Deglacial Indian monsoon failure and North Atlantic stadials linked by Indian Ocean surface cooling. Nat. Geosci. 9, 46–50. https://doi.org/10.1038/nego2603.
Trauth, M.H., Maslin, M.A., Deino, A.L., Junginger, A., Lesoloyia, M., Odada, E.O., Olago, D.O., Olaka, L.A., Strecker, M.R., Tiedemann, R., 2010. Human evolution in a variable environment: the amplifier lakes of Eastern Africa. Quat. Sci. Rev. 29, 2981–2988. https://doi.org/10.1016/J.QUASCIREV.2010.07.007.
Umer, M., Lamb, H.F., Bonnefille, R., Lézine, A.M., Tiercelin, J.J., Gibert, E., Cazet, J.P., Watrin, J., 2007. Late Pleistocene and Holocene vegetation history of the Bale Mountains, Ethiopia. Quat. Sci. Rev. 26, 2229–2246. https://doi.org/10.1016/J.QUASCIREV.2007.05.004.
Weldeab, S., Schneider, R.R., Kölling, M., Wefer, G., 2005. Holocene African droughts relate to eastern equatorial Atlantic cooling. Geology 33, 981–984. https://doi.org/10.1130/G21874.1.
Weldeab, S., Menke, V., Schmiedl, G., 2014. The pace of East African monsoon evolution during the Holocene. Geophys. Res. Lett. 41, 1724–1732. https://doi.org/10.1002/2014GL059361.
Zech, M., Glaser, B., 2009. Compound-specific δ18O analyses of neutral sugars in soils using gas chromatography-pyrolysis-isotope ratio mass spectrometry: problems, possible solutions and a first application. Rapid Commun. Mass Spectrom. 23, 3522–3532. https://doi.org/10.1002/rcm.4278.
Zech, M., Werner, R.A., Juchelka, D., Kalbitz, K., Buggle, B., Glaser, B., 2012. Absence of oxygen isotope fractionation/exchange of (hemi-) cellulose derived sugars during litter decomposition. Org. Geochem. 42, 1470–1475. https://doi.org/10.1016/J.ORGGEOCHEM.2011.06.006.
Zech, M., Tuthorn, M., Detsch, F., Rozanski, K., Zech, R., Zöller, L., Zech, W., Glaser, B., 2013. A 220 ka terrestrial δ18O and deuterium excess biomarker record from an eolian permafrost paleosol sequence, NE-Siberia. Chem. Geol. 360–361, 220–230. https://doi.org/10.1016/J.CHEMGEO.2013.10.023.
Zech, M., Mayr, C., Tuthorn, M., Leiber-Sauheitl, K., Glaser, B., 2014a. Reply to the comment of Sternberg on "Zech et al. (2014) Oxygen isotope ratios ($^{18}O/^{16}O$) of hemicellulose-derived sugar biomarkers in plants, soils and sediments as paleoclimate proxy I: Insight from a climate chamber experiment. GCA 126, 614–623". Geochim. Cosmochim. Acta 141, 680–682. https://doi.org/10.1016/j.gca.2014.05.048.
Zech, M., Tuthorn, M., Zech, R., Schlütz, F., Zech, W., Glaser, B., 2014b. A 16-ka δ18O record of lacustrine sugar biomarkers from the High Himalaya reflects Indian Summer Monsoon variability. J. Paleolimnol. 51, 241–251. https://doi.org/10.1007/s10933-013-9744-4.
Zhang, C., Ou, J., He, W., Huang, H., Cheng, G., Gu, Y., 2024. Optimisation Research on K-Means Clustering Algorithm Based on Principal Component Analysis and Percentile Improvement. 2024 6th International Conference on Artificial Intelligence and Computer Applications, ICAICA 2024, pp. 148–153. https://doi.org/10.1109/ICAICA63239.2024.10823007.